

Original Article

Docking-based structural splicing and reassembly strategy to develop novel deazapurine derivatives as potent B-Raf^{V600E} inhibitors

Gui-min WANG^{1,2,#}, Xiang WANG^{3,#}, Jian-ming ZHU^{1,#}, Bin-bin GUO^{1,2,#}, Zhuo YANG¹, Zhi-jian XU¹, Bo LI¹, He-yao WANG^{1,*}, Ling-hua MENG^{3,*}, Wei-liang ZHU^{1,*}, Jian DING³

¹CAS Key Laboratory of Receptor Research, Shanghai Institute of Materia Medica, Chinese Academy of Sciences, Shanghai 201203, China; ²University of Chinese Academy of Sciences, Beijing 100049, China; ³National Key Laboratory of Drug Research, Shanghai Institute of Materia Medica, Chinese Academy of Sciences, Shanghai 201203, China

Abstract

The mutation of B-Raf^{V600E} is widespread in a variety of human cancers. Its inhibitors vemurafenib and dabrafenib have been launched as drugs for treating unresectable melanoma, demonstrating that B-Raf^{V600E} is an ideal drug target. This study focused on developing novel B-Raf^{V600E} inhibitors as drug leads against various cancers with B-Raf^{V600E} mutation. Using molecular modeling approaches, 200 blockbuster drugs were spliced to generate 283 fragments followed by molecular docking to identify potent fragments. Molecular structures of potential inhibitors of B-Raf^{V600E} were then obtained by fragment reassembly followed by docking to predict the bioactivity of the reassembled molecules. The structures with high predicted bioactivity were synthesized, followed by *in vitro* study to identify potent B-Raf^{V600E} inhibitors. A highly potent fragment binding to the hinge area of B-Raf^{V600E} was identified via a docking-based structural splicing approach. Using the fragment, 14 novel structures were designed by structural reassembly, two of which were predicted to be as strong as marketed B-Raf^{V600E} inhibitors. Biological evaluation revealed that compound **1m** is a potent B-Raf^{V600E} inhibitor with an IC₅₀ value of 0.05 μmol/L, which was lower than that of vemurafenib (0.13 μmol/L). Moreover, the selectivity of **1m** against B-Raf^{WT} was enhanced compared with vemurafenib. In addition, **1m** exhibits desirable solubility, bioavailability and metabolic stability in *in vitro* assays. Thus, a highly potent and selective B-Raf^{V600E} inhibitor was designed via a docking-based structural splicing and reassembly strategy and was validated by medicinal synthesis and biological evaluation.

Keywords: B-Raf^{V600E} inhibitor; anticancer; vemurafenib; deazapurine; fragment reassembly; molecular docking; structure-activity relationship

Acta Pharmacologica Sinica advance online publication, 17 Apr 2017; doi: 10.1038/aps.2016.173

Introduction

The RAS-RAF-MEK-ERK signaling pathway is the most extensively characterized cascade of three mitogen-activated protein kinase (MAPK) pathways in the human body, which transduces the signals from extracellular spaces to intracellular locations and plays a prominent role in cell proliferation, differentiation and survival^[1-3]. Approximately one-third of human cancers possess mutations in this pathway^[3], among which the mutation of B-Raf^{V600E} has been identified in ~34%

of malignant melanoma^[4], ~58% of papillary thyroid cancer (PTC)^[5], 4.7% to 10% of colorectal cancer^[6,7], 12.5% of Grade 1 serous ovarian carcinoma^[8], ~94% of papillary craniopharyngioma^[9] and a wide variety of other cancers^[10]. Compared with other isoforms of the RAF kinase family, A-Raf and C-Raf (also known as Raf-1), the regulation of B-Raf activation requires less molecular events, resulting in increased kinase activity, and its activity is more frequently induced by a single point mutation^[11]. The B-Raf^{V600E} mutation has ~500-fold greater activity compared with wild type *in vitro*^[12]. Persistent B-Raf activation stimulates cancer cell proliferation and protects cells from apoptosis, which makes it an attractive anticancer drug target. B-Raf^{V600E} inhibitors have been heavily investigated by both academia and the pharmaceutical industry. Two small molecule drugs, vemurafenib (PLX4032, brand name: Zel-

These authors contributed equally to this work.

*To whom correspondence should be addressed.

E-mail wlzhu@simm.ac.cn (Wei-liang ZHU);

hywang@simm.ac.cn (He-yao WANG);

lhmeng@simm.ac.cn (Ling-hua MENG)

Received 2016-11-01 Accepted 2016-12-24

boraf) and dabrafenib (GSK2118436, brand name: Tafinlar), have been approved by the FDA for the treatment of multiple malignant cancers with the B-Raf^{V600E} mutation; thus, B-Raf^{V600E} is a novel anticancer drug target^[13-16]. There are some other B-Raf^{V600E} inhibitors in clinical trials or at various stages of drug development^[3]. However, new B-Raf^{V600E} inhibitors are still urgently required due to unaffordable cost and emerging resistance to present inhibitors^[16].

All protein kinases contain a segment connecting the amino- and carboxy-terminal kinase catalytic domain, known as the hinge region (Supplementary Figure S1), which could form hydrogen bonding interactions with the adenine ring of ATP, playing a central role in ATP-binding and substrate phosphorylation^[17, 18]. Accordingly, hindering ATP from binding to the hinge region should be a straightforward and effective approach to inhibit kinase activity. This approach has been confirmed by its use in numerous successful kinase inhibitors, *eg*, PD166326 (ABL1 inhibitor), axitinib (ABL1 and VEGFR2 inhibitor), lapatinib (EGFR and ERBB2 inhibitor), and sorafenib (a dual RAF-KDR inhibitor)^[18-20]. As a member of the kinase family, apart from the hinge region, the B-Raf catalytic area also includes a glycine-rich loop (G-loop), α C helix, and activation loop (A-loop) (Supplementary Figure S1)^[12]. To our knowledge, the vast majority of B-Raf^{V600E} inhibitors bind to the hinge region in kinase catalytic areas and overlap with the ATP-binding region to some extent. One or more critical hydrogen bonds are found between the hinge region of B-Raf^{V600E} and the inhibitors, which make a significant contribution to the binding affinity^[3, 15]. In accordance with the crystal structures of B-Raf^{V600E} and the drugs, both the 7-azaindole moiety of vemurafenib (PDB code: 3OG7^[13], Supplementary Figure S1B) and the 2-amino pyrimidine moiety of dabrafenib (PDB code: 4XV2^[15], Supplementary Figure S1D) form two critical hydrogen bonds with the hinge region, which greatly supports the central role of the hinge-binding area. In our previous work, combining pharmacophore-based virtual screening and scaffold hopping, a series of compounds were identified as B-Raf^{V600E} inhibitors. This study showed that forming strong hydrogen bonding with the hinge region results in enhanced IC₅₀ values for the series of inhibitors^[12].

Fragment-based drug discovery (FBDD) has been widely used in the pharmaceutical industry during recent years, typically as a mainstream alternative to high-throughput screening. With a high hit rate and satisfactory ligand efficiency (LE) of the hits, numerous inhibitors have advanced to clinical trials or have been approved using the FBDD approach^[21]. Vemurafenib is a remarkable representative of successful FBDD cases, which implies the applicability and high-efficiency of FBDD targeting B-Raf^{V600E}. The 7-azaindole moiety of vemurafenib was derived from high-concentration screening and was shown to form hydrogen bonding with the hinge area by crystallographic analysis. Another successful FBDD drug is the first approved PPI inhibitor Venetoclax (brand name: Venclexta), which was approved in April 2016 for the treatment of patients with chronic lymphocytic leukemia (CLL). Venetoclax was the first FDA-approved treatment that tar-

gets the B-cell lymphoma 2 (BCL-2) protein^[22]. In research, docking-based fragment screening and fragment reassembly, *ie*, fragment growing, fragment linking and fragment merging, were also applied and exhibited high efficiency in lead discovery and optimization^[23]. In addition to virtual screening programs, computational approaches have been developed to facilitate fragment reassembly. For instance, the AutoT&T2 software suite developed by Wang RX at the State Key Laboratory of Bioorganic and Natural Products Chemistry achieves automatic tailoring and transplanting with the hits from screening, which establishes a complete pipeline of FBDD and provides insight into *de novo* drug design^[24]. Accordingly, it is clear that appropriate application of FBDD could accelerate the drug discovery process.

In this context, we sought to identify a novel molecular fragment that can bind to the hinge region of B-Raf^{V600E} with high affinity and then performed further optimization using the FBDD strategy, as described in Figure 1.

Materials and methods

Fragment preparation, molecular docking and assembly

Molecular fragments were derived from the small molecular drugs listed in the top 200 pharmaceutical products by US retail sales in 2011. In consideration of the hinge-binding areas of vemurafenib and dabrafenib, we filtered the fragments generated by Pipeline Pilot 7.5 with the component named Generate Fragments using the following criteria: molecular weight ranges from 50 to 300 and number of heavy atoms ranges from 5 to 16^[25]. Molecular fragments were prepared using LigPrep with all possible protonation states generated at pH 7.0 \pm 3.0 by Epik^[26-28]. Then, Glide was utilized to perform molecular docking in its SP mode with the post-docking minimization including 10000 poses per ligand, and the remaining parameters were set to default. The X-ray structure of the B-Raf^{V600E} binding by vemurafenib (PDB code: 3OG7) was retrieved from the PDB as the docking structure in this study. To predict the binding modes of the new compounds, molecular docking was performed using Glide in its SP mode in a standard procedure^[29-31]. The docked conformations of the molecules with the lowest energy were selected for further studies.

Chemistry

All starting materials and solvents were purchased from commercial suppliers and used without further purification unless otherwise noted. The chemical synthesis of all the designed compounds is fully described in the Experimental Section of the Supplementary Information. The ¹H and ¹³C spectra were obtained on Bruker Avance III (Karlsruhe, Germany) with 300, 400, 500 and 600 NMR spectrometers operating at 300 MHz, 400 MHz or 600 MHz for ¹H NMR and 100 MHz or 125 MHz for ¹³C NMR, respectively. The deuterated solvents, such as CDCl₃ and DMSO-*d*₆, were used with the internal standard of tetramethylsilane (TMS). Chemical shifts are provided in δ values of ppm. The abbreviation s indicates singlet, d indicates doublet, t indicates triplet, and m indicates multiplet. Coupling constants (*J*) were measured in hertz (Hz). The

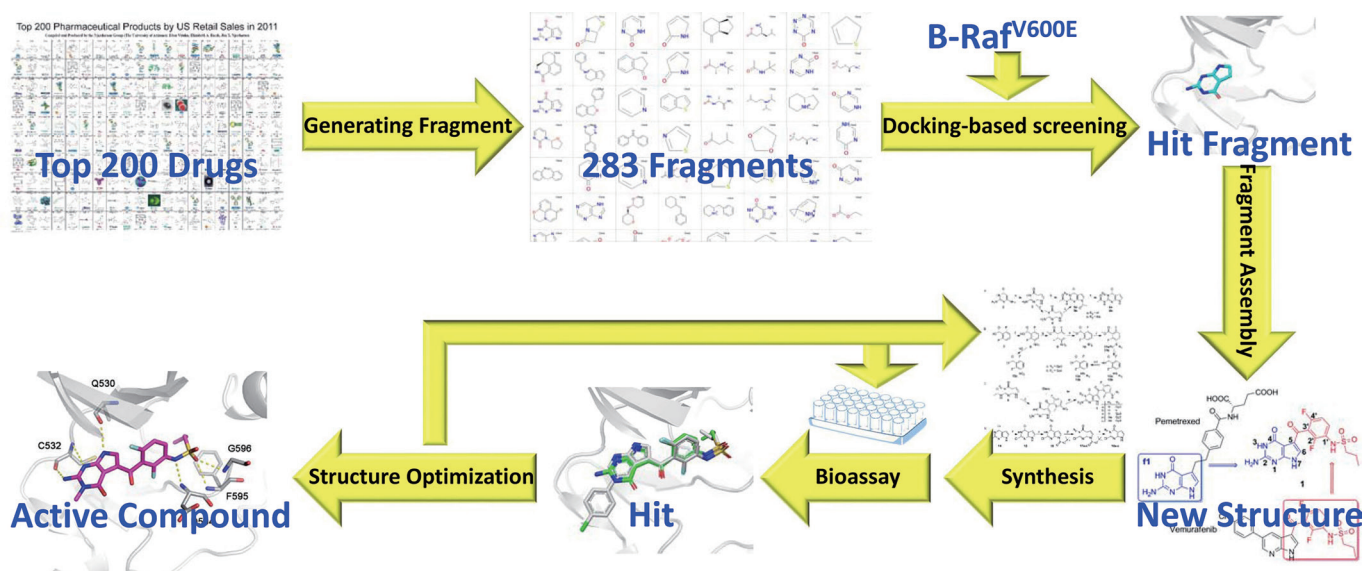


Figure 1. Schematic representation of the B-Raf^{V600E} inhibitor discovery process with FBDD.

LRMS and HRMS were recorded on a ThermoFinnigan LCQ Deca (San Jose, CA, USA) and a Micromass Q-TOF Ultima (in ESI mode, Manchester, UK) spectrometer, respectively.

Biological evaluation

Cell viability assessment

The human melanoma cell line A375 (B-Raf^{V600E}) and human colorectal cancer cell line HCT116 (B-Raf^{WT}) were used in the preliminary evaluation of the anti-tumor activity of the compounds using the MTT assay^[32]. The cells were dissociated into single suspension with H-DMEM culture medium containing 10% fetal bovine serum and then seeded into 96-well plates with 2500 (A375) or 3500 (HCT116) cells per well. After 24 h of cultivation, compounds were treated at the initial concentration of 10 $\mu\text{mol/L}$, and an equal amount of DMSO was used as the vehicle control. Cells were further incubated for 72 h, and then MTT solution was added to the well to a final concentration of 0.5 mg/mL. The plates were incubated at 37°C for 4 h. The medium was discarded, followed by addition of 100 μL DMSO. The plates were shaken for 10 min and absorbance was detected at 492 nm with a multi-well spectrophotometer.

The sulforhodamine B (SRB) staining assay was performed to detect the activity of compounds on the proliferation of HT-29, COLO205, LOVO, HCT-15, HCT-8, HCT116, SW1116, SW620 and SW480 human colorectal cancer cells. In brief, cells were seeded in 96-well plates at 3000 to 4000 cells/well, followed by treatment of serially diluted compounds for 72 h. The medium was replaced by 10% trichloroacetic acid, and then cells were stained with SRB. After cells being washed with 1% acetic acid, remaining SRB was dissolved in 100 μL of buffer containing 10 mmol/L Tris-base, and the OD value was measured at 560 nm with a multi-well spectrophotometer. The inhibitory rate of cell proliferation was calculated using the formula $(OD_{\text{control}} - OD_{\text{treatment}}) / OD_{\text{control}} \times 100\%$. The average

IC₅₀ values were from at least three independent tests.

In vitro B-Raf kinase assay

Given that B-Raf catalyzes the phosphorylation of MEK1/2, an ELISA-based MEK1/2 phosphorylation assay was developed and widely used in the evaluation of the kinase activity of B-Raf or the inhibitory activity of B-Raf inhibitors. To determine the IC₅₀ values of compounds in this study at the molecular level, we performed the ELISA-based MEK1/2 phosphorylation assay as previously described^[33]. A sigmoidal dose response curve was generated with duplicate or triplicate measurements at each inhibitor concentration using B-Raf^{V600E} or B-Raf^{WT} protein. Accordingly, IC₅₀ values were generated. In addition, Western blot assays were also performed to estimate the phosphorylation level of MEK1/2 using a standard procedure.

In vitro ADME profile and solubility

Human liver microsome assays were performed to evaluate *in vitro* metabolic stability. The concentrations of the parent compound in reaction systems were determined by LC-MS/MS to estimate the stability (the detailed experimental procedures and data analyses are included in the Supplementary Information). Solubility was measured in different buffer solutions using the classical shake test method. Permeability determination was performed using bidirectional permeability assays. In addition, metabolic evaluation with cytochrome P450 was also performed to assess the metabolic stability of the compound.

Results and discussion

Fragment generation and evaluation

Based on the structures of the top 200 drugs, 283 fragments were generated. Taking into account the different protonation states, 429 fragment structures were prepared for docking. All

of the fragment structures were then docked against B-Raf^{V600E} with one pose output for each structure (Supplementary Table S1). The top 10 fragments with the highest score (Figure 2) all formed hydrogen bonding with the hinge region, except for fragments **f3**, **f6** and **f7**. In particular, the fragment of pemetrexed (7-deazaguanine) **f1** with the highest docking score of -7.920 caught our attention given its 5 hydrogen bond acceptor/donors. We re-docked the fragment to B-Raf^{V600E} and output 3 poses to search for more binding modes. All 3 binding poses were located around the hinge region. Of note, in addition to the first pose with a docking score value of -7.920, the second pose, with a docking score of -7.603 and ligand efficiency (the docking score divided by the number of heavy (non-hydrogen) atoms) of -0.691, was predicted to superimpose well with the hinge-binding fragment of vemurafenib (Figure 3A). In addition, we also docked the hinge-binding fragment of vemurafenib, and the second conformation could reproduce the crystal structure of vemurafenib (Supplementary Figure S2). Impressively, the corresponding docking score (-7.742) is slightly lower than **f1** (-7.603), but the ligand efficiency (-0.484) is significantly increased compared with the latter (-0.691). Therefore, **f1** should be an ideal fragment to replace the 7-azaindole moiety of vemurafenib.

Hit compounds derived from fragment reassembly

Using **f1** as an ideal hinge-binding fragment, we sought to replace the hinge-binding area of vemurafenib with **f1**. To ensure the validity of the aforementioned fragment reassembly strategy, we performed molecular docking using the remaining vemurafenib moieties with the same parameters as the aforementioned fragment docking. As expected, the binding mode similar to that of vemurafenib was ranked third in the docking results with a docking score of -7.368 (Figure 3B). In this context, we found that no fragment apart from **f3** could bind to B-Raf^{V600E} at the same position with a higher docking score than -7.368. For synthesis, we replaced the 7-azaindole moiety of vemurafenib and obtained compound

1a (Figure 3C). The docking study revealed that **1a** is a potent inhibitor of B-Raf^{V600E} given its similar docking score and binding mode as vemurafenib (Table 1 and Figure 3D). Indeed, primary biological evaluation indicated that the IC₅₀ of **1a** was 0.80 μmol/L against the A375 cell line, whereas that of vemurafenib is 0.56 μmol/L. Given the availability of the reagents in our laboratory, compounds **1b-1n** were designed and synthesized for exploring the structure-activity relationship (Table 1). Among the new compounds, **1m** was predicted to have similar B-Raf^{V600E} inhibitory potential as **1a**.

Chemistry

The synthetic route of deazapurine derivatives studied in this study is outlined in Figure 4. 2-Bromo-1,1-dimethoxyethane was hydrolyzed under concentrated hydrochloride to obtain bromoacetaldehyde, which was then heated to condense 2,6-diaminopyrimidin-4(3H)-one (**2**) to give compound **3** under sodium acetate. Compound **3** was acetylated under acetic anhydride to obtain **5a**, which was then hydrolyzed to give **6a** under ammonium hydroxide without further purification. Compound **3** was methylated to obtain **4** under dimethyl sulfate, which was acetylated to achieve **6b** via **5b** (Figure 4A). 2,6-Difluorobenzoic acid (**7**) was nitrified to obtain **8** under the mixture of nitric acid and sulfuric acid, and **8** reacted with methanol under a catalytic amount of concentrated sulfuric acid to form **9**, which was reduced by iron powder in the solvent of acetic acid to obtain **10**. Then, **10** reacted with two equivalents of sulfonyl chloride to afford **11**, which was hydrolyzed under the aqueous solution of NaOH to achieve **12**. The derivatives of benzoic acid (**8**, **12a** and **12b**) were chloridized to afford the corresponding acyl chlorides (**13a-c**) (Figure 4B). Compounds **1a-d**, **1m** and **1n** were synthesized from the fragments obtained from procedures A and B (**6** and **13a-c**) via the Friedel-Crafts reaction in the presence of AlCl₃ (Figure 4C). Compound **14** was hydrolyzed by NaOH aqueous solution to achieve **15**, which was then protected by Boc to give **16**. Compounds **17a-c** were obtained by the reaction of **16**

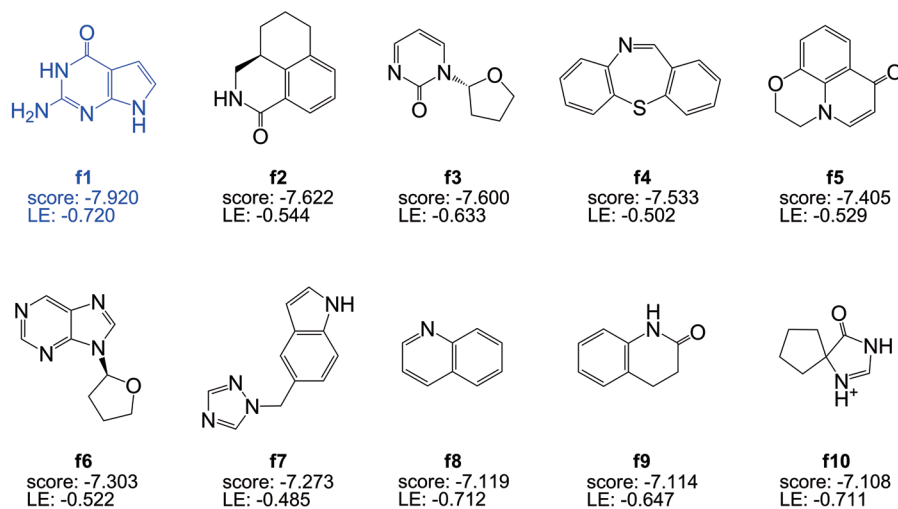


Figure 2. Structure of the top 10 molecular fragments ranked by docking score.

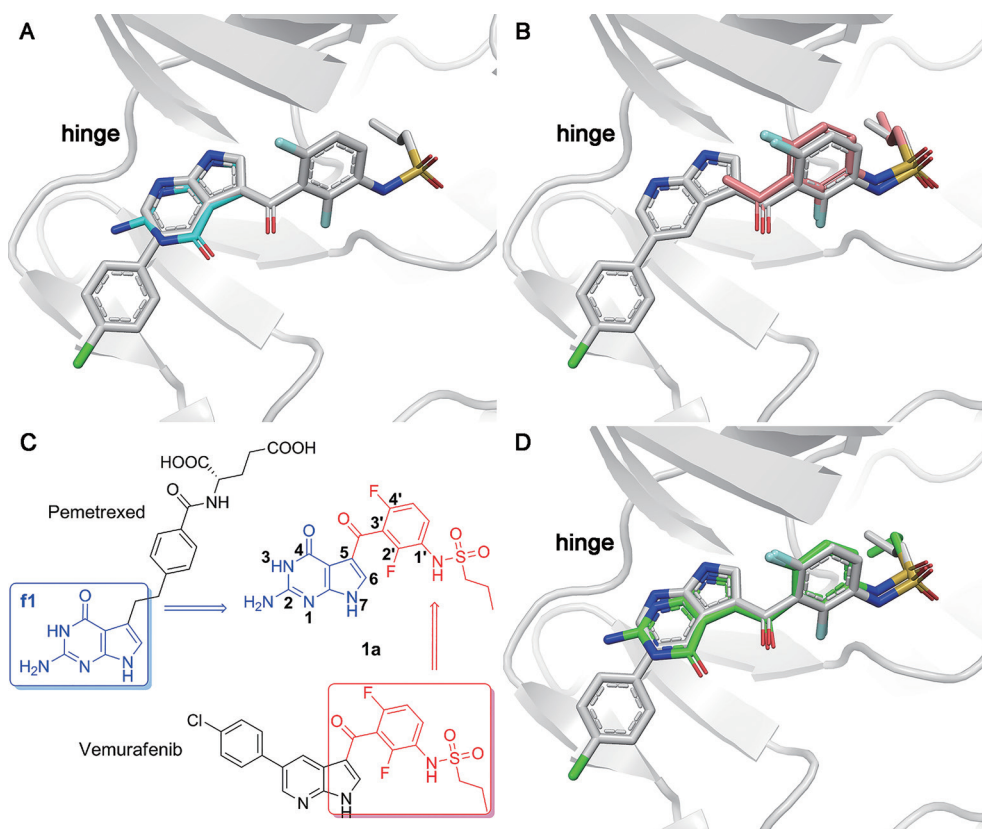


Figure 3. Molecular docking and fragment reassembly identified **1a** as a potential B-Raf^{V600E} inhibitor. Overlay of (A) **f1** (cyan), (B) hinge-binding fragment of vemurafenib (pink) and (D) **1a** (green) on vemurafenib (gray) with B-Raf^{V600E} (PDB entry 3OG7). The protein is shown in cartoon form and the ligands are in stick form. (C) Molecular tailoring and fragment reassembly.

with CH₃I, 4-nitrobenzyl bromide or allyl bromide, which was deprotected to give the important intermediates **18a-c** (Figure 4D). Compounds **1e-l** were synthesized from the fragments (**15** or **18a-c** and **13a-c**) obtained from the procedures B and D via the Friedel-Crafts reaction in the presence of AlCl₃ (Figure 4E).

Structure-activity relationship study

Vemurafenib forms 3 hydrogen bonds with residues D594, F595 and G596 by the sulfonamide moiety (Figure 5A). If **1a** interacts with B-Raf^{V600E} in a similar manner, replacing the sulfonamide moiety with amino (**1b**) should lead to loss of the inhibitory activity. The nitro substituted derivative **1c** exhibited weak inhibitory activity, but the selectivity against B-Raf^{WT} disappeared, which is consistent with the notion that the deprotonated sulfonamide favors an interaction with the B-Raf^{V600E} mutation other than the wild type^[34]. Using 2,6-difluorobenzenesulfonamido, the fragment of dabrafenib substituted at the 1'-position, **1d**, also exhibited weak inhibitory activity on A375 cells (Table 1).

Compared with vemurafenib, **1a** was predicted by a docking study to form one more hydrogen bond with C532 on the hinge region via the amino of 7-deazaguanine (Figure 5B). To explore how the hydrogen bonding contributes to the bind-

ing affinity, we replaced the amino groups of **1a**, **1b**, **1c** and **1d** with a chlorine atom, resulting in **1e**, **1f**, **1g** and **1h**, respectively. As expected, the activities of chlorine-substituted compounds became weaker compared with the amino-substituted compounds except for **1g**, whose inhibitory activity was extremely inconsistent with the docking score (Table 1). In view of the structure of **1g**, we hypothesized that the activity of **1g** in cells was not achieved by targeting B-Raf^{V600E} given that its selectivity between A375 and HCT116 cell lines was lost.

On account of the similar binding mode of **1a** and vemurafenib, increased substitution at the 3-position was proposed as rational (Figure 5D). From the organic synthetic perspective, methyl, allyl and 4-nitrobenzyl were added to **1e**, leading to **1i**, **1j** and **1k**, respectively. The activities of the three compounds were all improved compared with **1e**. Moreover, **1i** had the best performance with respect to both activity and selectivity. The methyl substituted derivative of **1h**, **1l**, also had a higher inhibition rate, implying that methyl substitution is applicable. Then, we synthesized two additional methyl-substituted derivatives, **1m** (Figure 5C) and **1n**. Compound **1n** exhibited increased activity against the A375 cell line compared with **1d**, whereas **1m** had the same IC₅₀ value as **1a** (0.80 μmol/L). At the molecular level, the IC₅₀ values of **1a** and **1m**

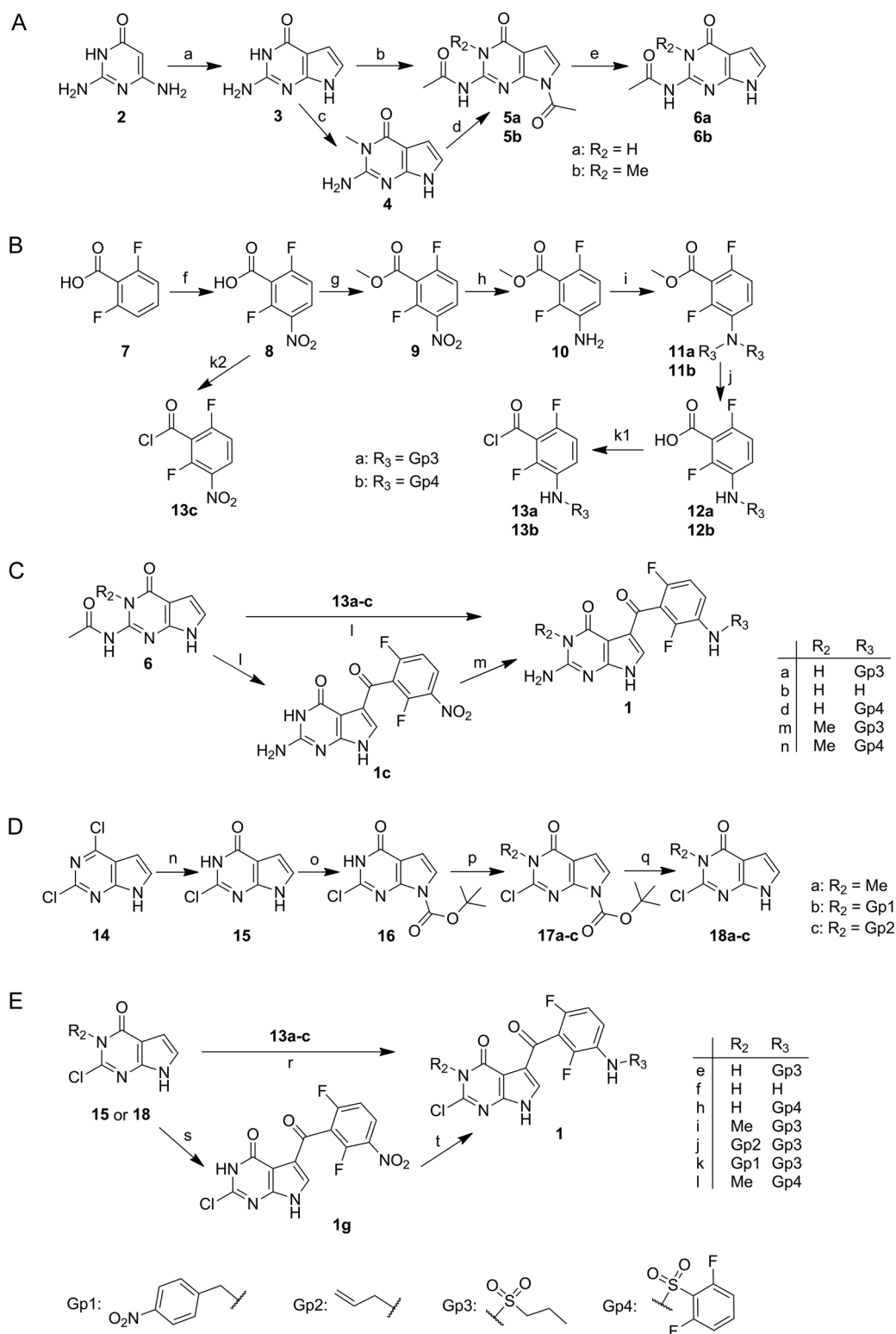


Figure 4. Synthesis of deazapurine derivatives. Reagents and conditions: (a) Bromoacetaldehyde dimethyl acetal, HCl, sodium acetate trihydrate, 80 °C, over night; (b) Acetic anhydride, acetic acid, 130 °C, 2 h; (c) 0.1 mol/L NaOH, dimethyl sulfate; (d) Acetic anhydride, acetic acid, 130 °C, 2 h; (e) Ammonium hydroxide, methanol; (f) 65%–68% HNO₃, H₂SO₄; (g) Conc sulfuric acid, methanol; (h) Acetic acid, ethanol, Fe powder, 110 °C, 0.5 h; (i) Triethylamine, 3-chloropropylsulfonyl chloride, 3.5 h; (j) NaOH (aq) THF, reflux, 2 h; (k1) SOCl₂, toluene, reflux, 3 h; (k2) Oxalyl chloride, cat. DMF, DCM; (l) AlCl₃, MeNO₂, 60 °C, 80–90 °C or 100–105 °C, over night; (m) Acetic acid, ethanol, Fe powder, 110 °C, 0.5 h; (n) NaOH (aq) 80 °C, over night; (o) Triethylamine, DMAP, Boc₂O, THF, RT, over night; (p1) KF, Mel, acetonitrile; (p2) Anhydrous DME and DMF, NaH, LiBr, 4-Nitrobenzyl bromide or allyl bromide; (q) Conc HCl, RT, over night; (r) AlCl₃, MeNO₂ or nitrobenzene, 60 °C, 80–90 °C or 100–105 °C, over night; (s) AlCl₃, MeNO₂, 60 °C, over night; (t) Acetic acid, ethanol, Fe powder, 110 °C, 0.5 h.

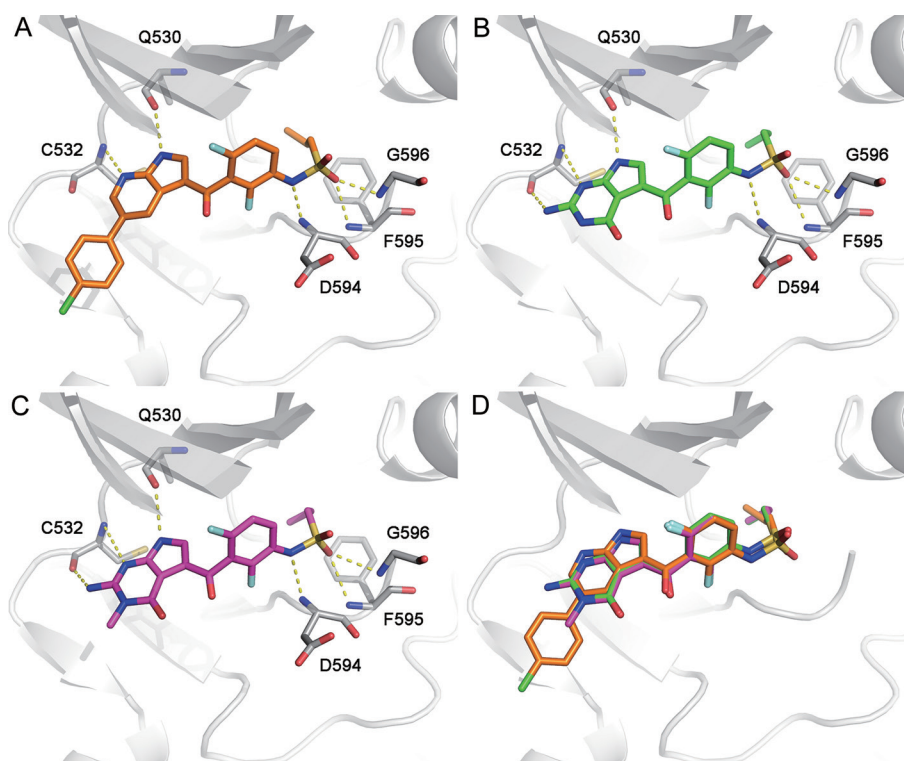


Figure 5. The binding mode of B-Raf^{V600E} inhibitors (docked with Glide in SP mode, PDB entry 3OG7). (A) Crystal structure of vemurafenib (orange) binding to B-Raf^{V600E}. (B) Predicted binding mode of **1a** (green) to B-Raf^{V600E}. (C) Predicted binding mode of **1m** (magenta) to B-Raf^{V600E}. (D) Superimposition view of all the three compounds. The protein is shown in cartoon form with critical residues and the inhibitors in stick form.

on B-Raf^{V600E} were 0.50 $\mu\text{mol/L}$ and 0.05 $\mu\text{mol/L}$, respectively, whereas that of vemurafenib was 0.13 $\mu\text{mol/L}$. In addition, the selectivity of **1m** (9 times) for B-Raf^{V600E} was increased compared with vemurafenib (5 times) against B-Raf^{WT} (Table 1). Accordingly, we obtained a potential B-Raf^{V600E} inhibitor with comparable activity and better selectivity than vemurafenib.

Assessment of **1m** against multiple colorectal cancer cell lines

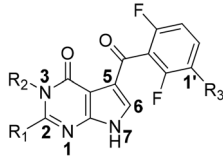
For the high proportion (4.7%–10%) of colorectal cancer patients bearing the B-Raf^{V600E} mutation, we used multiple colorectal cancer cell lines to evaluate the inhibitory activity and selectivity of **1m** (Table 2). The IC₅₀ values of **1m** were at the micromolar level in B-Raf^{V600E} mutant HT-29 and COLO205 cells, and these values were comparable to vemurafenib. However, the IC₅₀ values of **1m** were over 10 $\mu\text{mol/L}$ in LOVO, HCT-15, HCT-8, SW1116, HCT116, SW620 and SW480 cells, which harbor wild type B-Raf. The IC₅₀ values of vemurafenib in LOVO, HCT-15 and HCT-8 cells were 8.88 $\mu\text{mol/L}$, 7.75 $\mu\text{mol/L}$ and 5.84 $\mu\text{mol/L}$, respectively, indicating that **1m** exhibits superior selectivity against the V600E mutated cells compared with vemurafenib. A molecular docking study demonstrated that **1m** has a similar binding mode as vemurafenib. Furthermore, the sulfonamide moiety of vemurafenib is retained in **1m**, suggesting that the moiety preferred binding to the V600E mutant^[34], accounting for the selectivity of **1m**. In addition, the 7-deazaguanine moiety of **1m** forms more

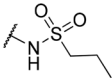
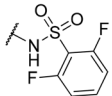
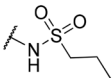
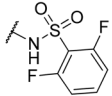
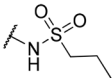
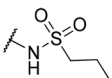
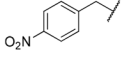
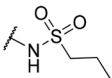
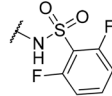
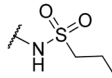
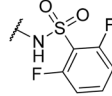
interactions with B-Raf^{V600E} than vemurafenib, which might be another reason why **1m** has lower activity against wild type B-Raf.

The phosphorylation level of MEK1/2, which are the downstream kinases of B-Raf, was determined in HT-29 cells to validate B-Raf^{V600E} inhibition by **1m** at the cellular level. After incubation with serially diluted **1m** or vemurafenib for 2 h, the phosphorylation level of MEK1/2 was measured by Western blot. Phosphorylated MEK1/2 significantly decreased with increasing concentrations of **1m** (Figure 6), confirming its target of B-Raf^{V600E} in HT29 cells. Similar observations were obtained with vemurafenib.

In vitro ADME properties

Finally, we determined the solubility, permeability and metabolic stability of **1m**. The human liver microsome assay indicated that the remaining rate (proportion of compounds that are not decomposed) of **1m** decreased slightly from 30 min to 2 h, implying that **1m** was stable in human liver microsomes (Supplementary Table S2 and Figure 7). Moreover, the metabolic stability evaluation concerning cytochrome P450 indicated that the metabolic bioavailability of **1m** was greater than 90% and varied slightly with different species. Furthermore, **1m** also exhibited good solubility, whereas the minimal soluble concentration of **1m** in buffers A and B was 50 $\mu\text{mol/L}$ and that in buffer C was 20 $\mu\text{mol/L}$. Regarding permeability,

Table 1. Structures, docking scores and biological activities of compounds.


No	R ₁	R ₂	R ₃	Docking score	Inhibition rate (%) at 10 μmol/L or IC ₅₀ (μmol/L)			
					A375	HCT116	B-Raf ^{V600E}	B-Raf ^{WT}
1a	NH ₂	H		-11.89	0.80	21% ^a	0.50	1.50
1b	NH ₂	H	NH ₂	-9.75	0.98%	-11.0%	NT	NT
1c	NH ₂	H	NO ₂	-10.29	9.13	6.71	NT	NT
1d	NH ₂	H		-10.85	19.08%	7.67%	NT	NT
1e	Cl	H		-9.46	-7.89%	-0.04%	NT	NT
1f	Cl	H	NH ₂	-7.43	-0.11%	-3.09%	NT	NT
1g	Cl	H	NO ₂	-7.47	4.69	4.68	NT	NT
1h	Cl	H		-8.81	-8.94%	-3.61%	NT	NT
1i	Cl	Me		-9.67	37.04%	5.32%	NT	NT
1j	Cl			-9.18	21.50%	1.49%	NT	NT
1k	Cl			-10.31	31.16%	21.34%	NT	NT
1l	Cl	Me		-8.90	16.93%	18.37%	NT	NT
1m	NH ₂	Me		-11.89	0.80	4.38%	0.05	0.44
1n	NH ₂	Me		-11.48	48.42%	19.26%	NT	NT
		Vemurafenib		-12.31	0.56	36.42	0.13	0.60
		Sorafenib		-7.25	10.01	8.70	NT	NT

^a Tested at 100 μmol/L.

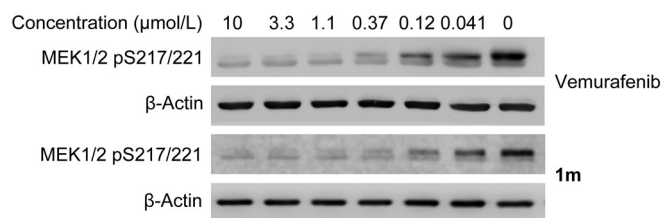
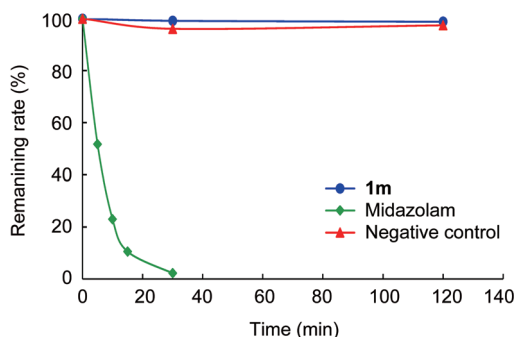
NT: Not test.

given that **1m** might be a substrate of P-gp (efflux ratio was 67.4), the *in vivo* absorption and bioavailability of **1m** should be higher than the *in vitro* predictive value (mean Fabs was

35%) for the saturation of the efflux transporter (Table 3). Accordingly, **1m** should have good ADME properties, including metabolism and bioavailability.

Table 2. The selectivity of **1m** for B-Raf^{V600E} over B-Raf^{WT} in multiple colorectal cancer cell lines.

B-Raf	Cell line	IC ₅₀ (μmol/L)	
		1m	Vemurafenib
V600E	HT-29	0.55±0.08	0.69±0.07
	COLO205	1.64±0.08	0.58±0.30
Wild type	LOVO	>10	8.88±2.50
	HCT-15	>10	7.75±0.10
	HCT-8	>10	5.84±1.53
	SW1116	>10	>10
	HCT116	>10	>10
	SW620	>10	>10
	SW480	>10	>10

**Figure 6.** The phosphorylation level of MEK1/2 in HT-29 cells was detected with Western blot.**Figure 7.** Metabolic stability of **1m** in human liver microsomes. Midazolam was a positive control and negative control was ultrapure-water rather than NADPH.**Table 3.** Solubility, permeability and metabolic stability of **1m**.

Buffer	Solubility		Permeability		Metabolic stability	
	Minimal soluble concentration (μmol/L)	Mean fabs (%)	Efflux ratio	Species	MF (%)	
A	50.0	35.0	67.4	Human	100	
B	50.0			Mouse	91	
C	20.0			Rat	90	

Buffer A: Hanks balanced salt solution (HBSS) buffer containing N-2-hydroxyethylpiperazine-N'-2-ethanesulfonic acid (HEPES) 10 mmol/L, pH 6.8 with bovine serum albumin (BSA) up to 0.1%.

Buffer B: HBSS buffer containing HEPES 10 mmol/L, pH 7.4 with BSA up to 0.1%.

Buffer C: TRIS buffer with BSA up to 0.1%.

Conclusion

In view of the structure and interaction analyses of approved drugs and inhibitors in development, we utilized molecular tailoring, molecular docking and fragment reassembly strategies to design and synthesize a series of deazapurine derivatives, among which compound **1m** was identified as a potential B-Raf^{V600E} inhibitor with comparable activity and superior selectivity compared with vemurafenib. Moreover, **1m** exhibits significant activity against the proliferation of HT-29 colorectal cancer cells harboring B-Raf^{V600E} with an IC₅₀ value of 0.55 μmol/L, which is lower than that of vemurafenib (0.69 μmol/L), while sparing B-Raf^{WT} cells (IC₅₀ >10 μmol/L). An obvious decrease in the phosphorylation of MEK1/2 was observed upon treatment with **1m**, confirming that **1m** inhibited B-Raf^{V600E} in cells. In addition, **1m** also exhibits good solubility, bioavailability and metabolic stability. These results of **1m** lay a solid foundation for further development. In addition, this study provides a novel strategy for designing inhibitors targeting B-Raf^{V600E}.

Acknowledgements

This work was supported by the National Natural Science Foundation of China (81273435, 81302699 and 81321092), the National Science and Technology Major Project (2013ZX09103001001), the Ministry of Science and Technology (2012AA01A305), the Natural Science Foundation of Shanghai, China (14ZR1447800), the State Key Laboratory of Natural and Biomimetic Drugs (K20150205) and the Special Program for Applied Research on Super Computation of the NSFC-Guangdong Joint Fund (the second phase).

Author contribution

Wei-liang ZHU, Bo LI, He-yao WANG, Ling-hua MENG, and Jian DING conceived and designed the research; Gui-min WANG, Xiang WANG, Jian-ming ZHU, Bin-bin GUO, and Zhuo YANG performed the research; Gui-min WANG, Xiang WANG, Jian-ming ZHU, Bin-bin GUO, and Zhi-jian XU analyzed the data; Gui-min WANG, Wei-liang ZHU, Jian-ming ZHU, Ling-hua MENG, and He-yao WANG wrote the paper.

Supplementary information

Supplementary information is available at the Acta Pharmacologica Sinica's website.

References

- 1 Li HF, Chen Y, Rao SS, Chen XM, Liu HC, Qin JH, et al. Recent advances in the research and development of B-Raf inhibitors. *Curr Med Chem* 2010; 17: 1618–34.
- 2 Maik-Rachline G, Seger R. The ERK cascade inhibitors: towards overcoming resistance. *Drug Resist Updates* 2016; 25: 1–12.
- 3 Uehling DE, Harris PA. Recent progress on MAP kinase pathway inhibitors. *Bioorg Med Chem Lett* 2015; 25: 4047–56.
- 4 Menzies AM, Haydu LE, Visintin L, Carlino MS, Howle JR, Thompson JF, et al. Distinguishing clinicopathologic features of patients with V600E and V600K BRAF-mutant metastatic melanoma. *Clin Cancer Res* 2012; 18: 3242–9.
- 5 Cancer Genome Atlas Research Network. Integrated genomic characterization of papillary thyroid carcinoma. *Cell* 2014; 159: 676–90.
- 6 Yokota T, Ura T, Shibata N, Takahari D, Shitara K, Nomura M, et al. BRAF mutation is a powerful prognostic factor in advanced and recurrent colorectal cancer. *Br J Cancer* 2011; 104: 856–62.
- 7 Fransen K, Klintenas M, Osterstrom A, Dimberg J, Monstein HJ, Soderkvist P. Mutation analysis of the BRAF, ARAF and RAF-1 genes in human colorectal adenocarcinomas. *Carcinogenesis* 2004; 25: 527–33.
- 8 DeFazio A, Moujaber T, Etemadmoghadam D, Kennedy C, Chiew YE, Balleine RL, et al. Abstract A25: BRAF^{V600E} mutations in serous ovarian cancer and response to the BRAF inhibitor, dabrafenib. *Clin Cancer Res* 2016; 22: A25.
- 9 Brastianos PK, Taylor-Weiner A, Manley PE, Jones RT, Dias-Santagata D, Thorner AR, et al. Exome sequencing identifies BRAF mutations in papillary craniopharyngiomas. *Nat Genet* 2014; 46: 161–5.
- 10 Fiskus W, Mitsiades N. B-Raf inhibition in the clinic: present and future. *Annu Rev Med* 2016; 67: 29–43.
- 11 Qin J, Xie P, Ventocilla C, Zhou G, Vultur A, Chen Q, et al. Identification of a novel family of BRAF^{V600E} inhibitors. *J Med Chem* 2012; 55: 5220–30.
- 12 Xu Z, Yan G, Wang G, Li B, Zhu J, Sun P, et al. Combining pharmacophore, docking and substructure search approaches to identify and optimize novel B-Raf^{V600E} inhibitors. *Bioorg Med Chem Lett* 2012; 22: 5428–37.
- 13 Bollag G, Hirth P, Tsai J, Zhang J, Ibrahim PN, Cho H, et al. Clinical efficacy of a RAF inhibitor needs broad target blockade in BRAF-mutant melanoma. *Nature* 2010; 467: 596–9.
- 14 Flaherty KT, Yasothan U, Kirkpatrick P. Vemurafenib. *Nat Rev Drug Discov* 2011; 10: 811–2.
- 15 Zhang C, Spevak W, Zhang Y, Burton EA, Ma Y, Habets G, et al. RAF inhibitors that evade paradoxical MAPK pathway activation. *Nature* 2015; 526: 583–6.
- 16 Sun XX, Yu Q. Intra-tumor heterogeneity of cancer cells and its implications for cancer treatment. *Acta Pharmacol Sin* 2015; 36: 1219–27.
- 17 Akritopoulou-Zanze I, Hajduk PJ. Kinase-targeted libraries: the design and synthesis of novel, potent, and selective kinase inhibitors. *Drug Discov Today* 2009; 14: 291–7.
- 18 Zhang J, Yang PL, Gray NS. Targeting cancer with small molecule kinase inhibitors. *Nat Rev Cancer* 2009; 9: 28–39.
- 19 Hoi PM, Li S, Vong CT, Tseng HH, Kwan YW, Lee SM. Recent advances in structure-based drug design and virtual screening of VEGFR tyrosine kinase inhibitors. *Methods* 2015; 71: 85–91.
- 20 Pemovska T, Johnson E, Kontro M, Repasky GA, Chen J, Wells P, et al. Axitinib effectively inhibits BCR-ABL1(T315I) with a distinct binding conformation. *Nature* 2015; 519: 102–5.
- 21 Kumar A, Voet A, Zhang KY. Fragment based drug design: from experimental to computational approaches. *Curr Med Chem* 2012; 19: 5128–47.
- 22 Roberts AW, Davids MS, Pagel JM, Kahl BS, Puvvada SD, Gerecitano JF, et al. Targeting BCL2 with venetoclax in relapsed chronic lymphocytic leukemia. *N Engl J Med* 2016; 374: 311–22.
- 23 Joseph-McCarthy D, Campbell AJ, Kern G, Moustakas D. Fragment-based lead discovery and design. *J Chem Inf Model* 2014; 54: 693–704.
- 24 Radoux CJ, Olsson TS, Pitt WR, Groom CR, Blundell TL. Identifying interactions that determine fragment binding at protein hotspots. *J Med Chem* 2016; 59: 4314–25.
- 25 Pipeline Pilot; Accelrys Software Inc: San Diego, CA, USA.
- 26 LigPrep, version 2.4, Schrödinger, LLC: New York, NY, USA, 2010.
- 27 Epik, version 2.1; Schrodinger, LLC: New York, NY, USA, 2010.
- 28 Shelley JC, Cholleti A, Frye LL, Greenwood JR, Timlin MR, Uchimaya M. Epik: a software program for pK_a prediction and protonation state generation for drug-like molecules. *J Comput Aided Mol Des* 2007; 21: 681–91.
- 29 Friesner RA, Banks JL, Murphy RB, Halgren TA, Klicic JJ, Mainz DT, et al. Glide: a new approach for rapid, accurate docking and scoring. 1. Method and assessment of docking accuracy. *J Med Chem* 2004; 47: 1739–49.
- 30 Halgren TA, Murphy RB, Friesner RA, Beard HS, Frye LL, Pollard WT, et al. Glide: a new approach for rapid, accurate docking and scoring. 2. Enrichment factors in database screening. *J Med Chem* 2004; 47: 1750–9.
- 31 Friesner RA, Murphy RB, Repasky MP, Frye LL, Greenwood JR, Halgren TA, et al. Extra precision glide: docking and scoring incorporating a model of hydrophobic enclosure for protein-ligand complexes. *J Med Chem* 2006; 49: 6177–96.
- 32 Tolosa L, Donato MT, Gomez-Lechon MJ. General cytotoxicity assessment by means of the MTT assay. *Methods Mol Biol* 2015; 1250: 333–48.
- 33 Xie P, Streu C, Qin J, Bregman H, Pagano N, Meggers E, et al. The crystal structure of BRAF in complex with an organoruthenium inhibitor reveals a mechanism for inhibition of an active form of BRAF kinase. *Biochemistry* 2009; 48: 5187–98.
- 34 Tsai J, Lee JT, Wang W, Zhang J, Cho H, Mamo S, et al. Discovery of a selective inhibitor of oncogenic B-Raf kinase with potent anti-melanoma activity. *Proc Natl Acad Sci U S A* 2008; 105: 3041–6.